**RAA 2016** Vol. **16** No. **1**, 4 (8pp) doi: 10.1088/1674–4527/16/1/004
*http://www.raa-journal.org* *http://iopscience.iop.org/raa*

***R**esearch in*
***A**stronomy and*
***A**strophysics*

# Global Mg/Si and Al/Si Distributions on the Lunar Surface Derived from Chang'E-2 X-ray Spectrometer

Wu-Dong Dong, Xiao-Ping Zhang, Meng-Hua Zhu, Ao-Ao Xu and Ze-Sheng Tang

Lunar and Planetary Science Laboratory, Macau University of Science and Technology, Macao, China;
*xpzhang@must.edu.mo, dowudong@gmail.com*

Received 2014 November 28; accepted 2015 July 29

**Abstract** The technique of X-ray fluorescence remote sensing plays a significant role in research related to the chemical compositions of the Moon. Here we describe the data analysis method for China's Chang'E-2 X-ray spectrometer in detail and present the preliminary results about the first global Mg/Si and Al/Si maps of the lunar surface. Our results show that the distributions of Mg/Si and Al/Si correlate well with terrains on the Moon. The higher Mg/Si ratio corresponds to the mare regions while the lower value corresponds to the highland terrains. The map of the Al/Si ratio shows a reversed distribution compared with the map of the Mg/Si ratio.

**Key words:** Moon — planets and satellites: composition — techniques: spectroscopic — X-rays: general

## 1 INTRODUCTION

Chemical compositions on the lunar surface are critical in the determination of the geochemical nature of lunar terrains and the geologic evolution history of the Moon. X-ray spectroscopy is considered to be one of the most effective methods among all remote sensing techniques to study the major element abundances on an airless planetary surface, such as the Moon, Mercury and asteroids (Adler et al. 1973; Clark & Trombka 1997; Trombka et al. 2000; Grande et al. 2003; Sun et al. 2008; Nittler et al. 2011). In this technique, solar X-rays interact with materials on the planet's surface producing characteristic X-ray fluorescences at the uppermost surface layer. The characteristic fluorescent X-rays of major elements, such as K$\alpha$ lines of Mg (1.254 keV), Al (1.487 keV), Si (1.740 keV), Ca (3.692 keV), Ti (4.511 keV) and Fe (6.404 keV), can be detected by instruments in orbit.

X-ray spectrometers have been carried on many spacecrafts in the past. The X-ray spectrometer onboard the Soviet Luna 12 orbiter, launched in 1966, first successfully observed fluorescent X-rays from the Moon (Mandel'Shtam et al. 1968). Later in 1971–1972, X-ray fluorescences were measured by proportional counters in the lunar equatorial region of the nearside in Apollo 15 and 16 missions, covering $\sim 10\%$ of the global lunar surface. For many years, this data set was the only observation of the large-scale chemical compositions of the lunar surface from an X-ray spectrometer. The Al/Si and Mg/Si ratios were derived from Apollo X-ray Spectrometer data, providing a preliminary understanding of the distribution of the local feature of chemical composition distributions on the lunar surface (Adler et al. 1972a,b; Clark 1979). The Demonstration of a Compact Imaging X-ray Spectrometer (D-CIXS) payload onboard SMART-1 launched by ESA in 2003 detected characteristic X-ray lines from rock-forming elements during several solar flare events (Grande et al. 2003; Grande et al. 2007; Swinyard et al. 2009). Unfortunately, the detector suffered severe damage from radiation in orbit during its observation, and no accurate quantitative analysis could be performed. The X-ray spectrometer onboard the Kaguya spacecraft that was launched in 2007 also suffered the same problem (Yamamoto et al. 2008; Okada et al. 2009). The X-ray spectrometers onboard the first Chinese lunar spacecraft Chang'E-1 launched in 2007 (Sun et al. 2008; Ouyang et al. 2008; Ouyang et al. 2010a,b) and Indian Chandrayaan-1 launched in 2008 (Grande et al. 2009) successfully detected fluorescent X-rays from rock-forming elements (Ouyang et al. 2008; Peng 2009; Narendranath et al. 2011; Weider et al. 2012, 2014). Since the Sun was in a quiescent period at that time, solar flares were few and the incident X-ray intensity was not powerful enough. As a result, the data were not sufficient for producing a global elemental distribution map.

The Chang'E-2 (CE-2) spacecraft, which was China's second unmanned lunar probe, was successfully launched on 2010 October 1. An innovative X-ray instrument named the Chang'E-2 X-ray spectrometer (CE2XRS) was onboard CE-2. Ban et al. (2014) derived the elemental abundances of Mg, Al, Si, Ca and Fe in the lunar Oceanus Procellarum region using CE2XRS data acquired during an M-class solar flare event. However, there has been no global elemental abundance map of the Moon from an X-ray spectrometer until now. Fortunately, the Sun was in its active period so a number of solar flare events were ob-

served during the CE-2 mission. After more than half a year of observations, large amounts of scientific data were obtained by CE2XRS. It is, therefore, the best opportunity to derive the first global chemical composition maps of major elements with CE2XRS.

In this paper, we describe the data analysis procedure and present the global Mg/Si and Al/Si distributions on the lunar surface derived from CE2XRS data. This is the first global map derived by remote X-ray fluorescence spectroscopy on the Moon. Lunar global geochemical features are discussed based on the elemental distribution maps. Three major geological units on the Moon (lunar mare, highland and the South Pole-Aitken (SPA) basin) are identified.

In Section 2, we give a brief description of the CE2XRS. In Section 3, we describe the primary data processing that includes the data check, data selection, background determination, spectral deconvolution and elemental abundance mapping. Finally, in Section 4, we make a comparison between the global map of Mg/Si and Al/Si molar ratio distribution on lunar surface derived from CE2XRS and LPGRS. In adittion, we give possible reasons to explain their differences.

## 2 CHANG'E-2 X-RAY SPECTROMETER

The X-ray spectrometer, one of the scientific payloads onboard the CE-2 spacecraft, was intended to obtain the distributions of major rock-forming elements (i.e., Mg, Al, Si, Ca, Ti and Fe) on the Moon. Since the detailed structure and specification of CE2XRS have been presented by Peng et al. (2009) and Ban et al. (2014), we only give a brief description here.

The CE2XRS was designed to be a compact detector. It consisted of a lunar X-ray detector, solar X-ray monitor and electronics box (see Fig. 1), which were improved compared to the X-ray spectrometer on the Chang'E-1 spacecraft. A pair of orthogonal collimators made of a permanent magnets limited the field of view of the detectors to have an optimal spatial resolution of $\sim$200 km $\times$ 70 km at a distance of 100 km from the lunar surface. The layout of the detectors and collimators was described by Peng et al. (2009). The lunar X-ray detector was designed to measure lunar fluorescent X-rays. It was composed of a soft X-ray detector array (SXDA) and a hard X-ray detector array (HXDA). The SXDA had four Si-PIN detectors identified as 1111–9, 1111–10, 2222–9 and 2222–10. The detectable energy range of SXDA was 0.5–10 keV and the energy resolution was 300 eV@5.95 keV. For HXDA, the detectable energy range was 25–60 keV and the energy resolution was 6.0 keV@59.5 keV. The solar X-ray monitor (SXM) had a small Si-PIN detector. It was the same as the detector in SXDA except for the effective detector area. The SXM was designed to simultaneously measure the solar X-ray spectrum. A $^{55}$Fe radioactive source attached to the 1111–9 detector in SXDA was used to calibrate the instrument in orbit. X-rays emitted from the $^{55}$Fe source generated the Mn K$\alpha$ and K$\beta$ lines at 5.898 keV and 6.490 keV, respectively. The instrumental specifications of the X-ray spectrometer are listed in Table 1.

## 3 CE2XRS DATA ANALYSIS

The CE-2 spacecraft followed a polar orbit with a period of $\sim$ 118 minutes at an average altitude of 100 km. There were 2739 orbits of data collected from 2010 October 15 to 2011 May 20. In our analysis, we use the CE2XRS level 2C dataset and only analyze the data from detector 1111–9 in SXDA. The data format is shown in Table 2. The description of the dataset was presented by Ban et al. (2014). A general data analysis method for the X-ray spectrometer was published by Clark & Trombka (1997), Starr et al. (2000) and Peng (2009). Here we describe the CE2XRS data analysis method for the global elemental distribution map in detail.

### 3.1 Data Check

For the CE2XRS level 2C data, there is a label "quality_state" (see Table 2) appended to the end of each record. A value of "quality_state" equaling "00" (decimal value = 0) indicates that the record is good. If a record label "quality_state" is not equal to "00," this record is eliminated (see Fig. 2). The label "distance" is the altitude between the CE-2 spacecraft and the lunar surface. The normal average working altitude of CE2XRS is $\sim$100 km. The records with the value labeled "distance" greater than 125 km are deleted (see Fig. 3), although the percentage of such measurements is very low.

Also, we check the relationship between channel number and energy for the detector 1111–9. This detector has 1024 channels. The channel information is stored in the level 2B dataset. The level 2C dataset is generated when the channel-energy calibration was carried out on the level 2B dataset. This preliminary calibration was made by the Institute of High Energy Physics and National Astronomical Observatories. We find a good linear relationship between channel number and energy (see Fig. 4) which demonstrates the good quality of the CE2XRS data. After the data check is finished, the final corrected data are ready for spectral analysis.

### 3.2 The Solar Activity and Data Selection

Solar X-rays are the primary excitation sources for the generation of fluorescent X-rays from the lunar surface. When the Sun is in an active period, the solar X-ray flux significantly increases. The flux of higher energy X-rays may increase several orders of magnitude and makes the solar X-ray spectra much harder during a solar flare. Hence, fluorescent X-rays from the lunar surface greatly increase and the signal-to-noise ratio also goes up in this period. When the Sun is in a quiescent period, the fluorescent X-rays are much lower and much more data accumulation time is needed to achieve significant results. The relationship be-

**Fig. 1** The CE2XRS instruments, listed from left to right, are the electronic box, solar X-ray monitor and lunar X-ray detector. The photograph is from Peng et al. (2009).

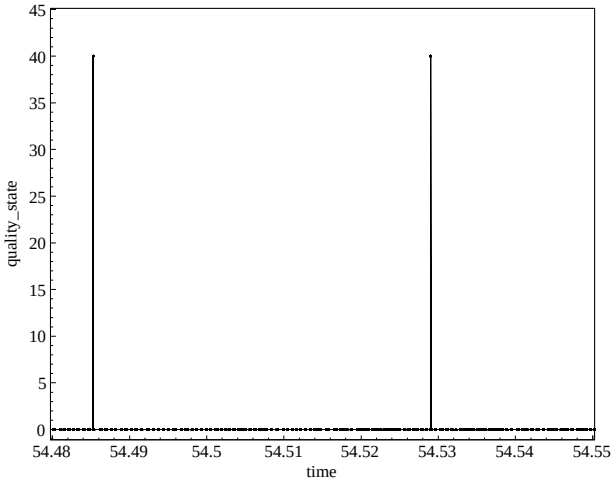


**Fig. 2** The scatter plot of label "quality_state" versus time from the data in orbit number 578. The time means the number of days since 2010 October 1. This orbital record represents the time span from 11:22 to 13:20 on 2010 November 24 (UTC). The bad record with the "quality_state" of "40" happened at 11:38 and 12:41. These abnormal records are eliminated in the data check process.

**Table 1** Technical Specifications of CE2XRS from Peng et al. (2009)

| Component | SXD | HXD | SXM |
|---|---|---|---|
| Detector | Si-PIN (4 chips) | Si-PIN (16 chips) | Si-PIN (1 chip) |
| Filter | 12.5 μm Be | 1 μm Al | 12.5 μm Be |
| Effective area | 1 $cm^2$ | 16 $cm^2$ | 0.2 $mm^2$ |
| Detectable range | 0.5–10 keV | 25–60 keV | 0.5–10 keV |
| Energy resolution | 300 eV@5.9 keV | 6 keV@59.5 keV | 300 eV@5.9 keV |

tween the variation in solar activity and the intensity of fluorescent X-rays was derived by Clark & Trombka (1997).

In our analysis, the solar plasma temperature ($T_{\rm solar}$) parameter is used to represent the intensity of solar activity. We adopt the solar plasma isothermal model to derive the solar plasma temperature. The solar X-ray flux data are taken from the Geostationary Operational Environmental Satellite (GOES). GOES measures the solar flux in two channels (1–8 Å and 0.5–4 Å, corresponding to energies of 1.55–12.4 keV and 3.1–24.8 keV respectively) simultaneously every 3 s. Thomas et al. (1985) and Garcia (1994) have published methods for calculating solar plasma temperature from GOES data. This model was used by Trombka et al. (2000) and Nittler et al. (2001) in the NEAR-Shoemaker XRS papers to interpret the elemental composition of asteroid 433 Eros and was also adopted in CE-1 XRS data analysis by Peng (2009). The relationship between solar plasma temperature and the solar flux ratio (SFR) was obtained by a fitting method (Peng 2009). The SFR is defined by the ratio of flux in channel 1–8 Å to the flux in channel 0.5–4 Å. When the SFR increases, the solar plasma temperature goes down.

**Table 2** The Format of the CE2XRS Level 2C Dataset

| Column | Label | Column | Label |
|---|---|---|---|
| 1 | time | 7 | instrument_azimuth_angle_2 |
| 2 | longitude | 8 | solar_incidence_angle |
| 3 | latitude | 9 | detector_number |
| 4 | distance | 10 | energy |
| 5 | instrument_incidence_angle | 11 | counts |
| 6 | instrument_azimuth_angle | 12 | quality_state |

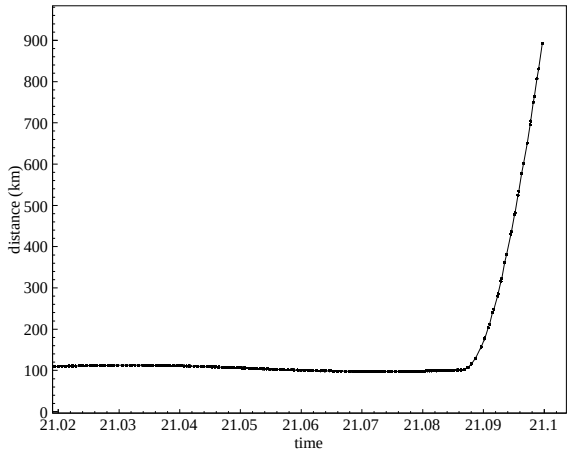


**Fig. 3** The scatter plot of label "distance" versus time from the data in orbit number 169. The time means the number of days since 2010 October 1. This orbital record represents the time span from 00:25 to 02:23 on 2010 October 22 (UTC). The "distance" (altitude of the orbit) sharply increased at 02:07. These records are removed because the CE-2 spacecraft might have been doing an orbital transfer at that time.

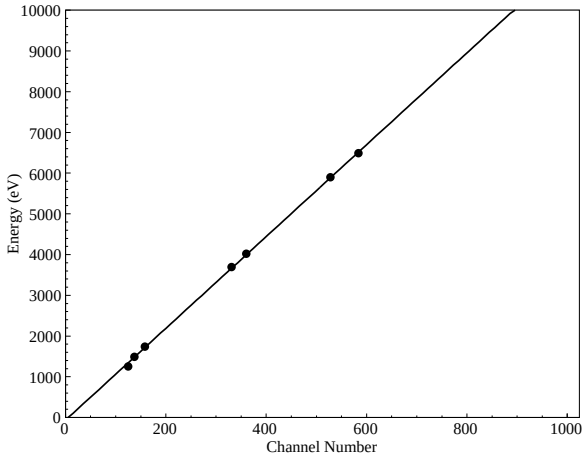


**Fig. 4** The linear relationship between channel number and energy from detector 1111–9 data. The points from left to right are Mg(K$\alpha$), Al(K$\alpha$), Si(K$\alpha$), Ca(K$\alpha$), Ca(K$\beta$), Mn(K$\alpha$) and Mn(K$\beta$).

From the GOES solar flare event report[1], we find that there were many solar flare events during the CE2XRS observation period from 2010 October 15 to 2011 May 20. For the solar flare event with level B and above, the footprint of CE2XRS on the Moon covered the whole lunar surface. The level of solar activity was good for mapping major elements, such as Mg, Al and Si, on the entire lunar surface. To obtain statistically significant results for globally mapping, X-ray spectra with the same level of solar activity and at the same location are accumulated. To increase the signal-to-noise ratio, only the data acquired in the sunlit side of the Moon with solar incidence angle less

[1] *http://www.ngdc.noaa.gov/stp/space-weather/solar-data/solar-features/solar-flares/x-rays/goes/*

than $88^\circ$ are accumulated. The final data are categorized by different solar plasma temperatures. We find the amount of data with a solar plasma temperature of 4 MK is sufficient for deriving a global distribution map of Mg, Al and Si on the entire lunar surface. Therefore, this level of solar activity is selected for our analysis. Hereafter, all operations are done on the data at this level of solar activity.

The lunar surface is partitioned into a series of equal area grids for mapping CE2XRS data. According to the spatial resolution of CE2XRS and the statistics of the data, the grid size is set to be $20^\circ \times 20^\circ$. The partitioned grids start at the lunar equator and continue to the polar regions with the same latitude intervals but different longitude intervals. The total number of grids is 114. All corrected data in the same grid and at the same level of solar activity are accumulated to form a set of spectra that can be used in further analysis.

### 3.3 Background Determination

The X-rays detected by CE2XRS in orbit include not only the fluorescent X-rays from the lunar surface, but also the backgrounds which come from internal electronic noise of the instrument (Peng 2009), external cosmic ray induced background and scattered solar X-rays (Nittler et al. 2001). Ban et al. (2014) made a comparison of the electronic noise background at different temperatures. It was found that the electronic noise of the detector was fairly constant and changed slightly with the detector's temperature. The overall shape of the cosmic ray induced background spectra also tends to be constant over a timescale of a few hours, but the magnitude varies (Lim & Nittler 2009; Nittler et al. 2011; Narendranath et al. 2011). In our analysis, the internal electronic noise and cosmic ray induced background are determined by summing over all measurements in the same level of solar activity and on the dark side of the Moon. This method for background determination was widely adopted by many investigators (Clark & Trombka 1997; Peng 2009; Nittler et al. 2011; Narendranath et al. 2011; Weider et al. 2012; Ban et al. 2014). Ban et al. (2014) used the dark side with solar incident angle larger than $90^\circ$ as the background. To avoid direct illuminations of light from the Sun or zodiacal light on the detector near the terminator, only the spectra with a solar X-ray incident angle greater than $120^\circ$ are added for background determination in our analysis. In our case, the background variation with incident angle larger than $120^\circ$ is more stable as a function of incident angle. Then, the background is normalized according to the accumulation time and directly subtracted from the spectra acquired from the sunlit side of the Moon.

Figure 5 shows example spectra observed by CE2XRS from both the sunlit side and the dark side with solar incident angles larger than $120^\circ$ when $T_{\rm solar} = 4$ MK. The scattered solar X-ray background on the sunlit side has been calculated theoretically by Clark & Trombka (1997). Nittler et al. (2001) used this method to predict scattered solar X-ray spectra at different solar plasma temperatures. The shape in the low energy part of the scattered solar X-ray spectra is approximately a Gaussian profile at low solar plasma temperature. Therefore we use a Gaussian function to model the spectra from the scattered solar X-ray background. As shown in the following subsection, this function describes the low energy tail of the spectra well.

### 3.4 Spectral Deconvolution and Elemental Abundance Mapping

After the electronic noise and cosmic ray induced background were subtracted, the residual spectra were deconvolved to obtain the flux of each major element, such as Mg, Al and Si. For most spectra, the fitting function is the sum of three normalized Gaussian functions for Mg, Al and Si, respectively, and a Gaussian function for the scattered solar X-ray background (see Fig. 6). Each element intensity is determined by the best fit of the spectra with a minimum $\chi^2$ method that takes into account the error bar of each data point. The fitting procedure is coded and implemented in ROOT[2] software. One can also obtain the uncertainties of the X-ray flux of each element from the fitting results. Based on the fitting results, we derived the X-ray intensity ratio for each element relative to Si. Si abundances only vary slightly on the lunar surface. In the analysis, ratioing to Si helps to remove matrix effects that come from compositional variations in the lunar regolith and from geometric corrections (Clark & Trombka 1997). Then, the elemental flux ratios are used to create global distribution maps on the lunar surface.

## 4 RESULTS AND DISCUSSIONS

After the above data processing steps are carried out, we obtain the first global Mg/Si and Al/Si maps of the Moon derived from CE2XRS level 2C data under the solar condition of temperature $T = 4$ MK derived from the solar plasma isothermal model (Garcia 1994). The result is normalized by global Mg/Si and Al/Si data derived from the Gamma Ray Spectrometer on Lunar Prospector (LPGRS) (Prettyman et al. 2006).

Figure 7 shows the global Mg/Si map with a resolution of $20^\circ \times 20^\circ$ and the same resolution map from LPGRS. Figure 8 shows the global Al/Si map with a resolution of $20^\circ \times 20^\circ$ and the same resolution map from LPGRS. From Figure 7, we can find that the high Mg/Si ratios are mainly concentrated at the Procellarum KREEP Terrane (PKT) and SPA basin while Feldspathic Highlands Terrane (FHT) has a low value. However, the high Al/Si ratios show a reversed distribution at the FHT with a low value at PKT and SPA, as shown in Figure 8. All these maps are nicely consistent with the maps derived from LPGRS.

The possible reasons for the differences in certain regions of elemental abundance ratios derived between

[2] The ROOT software can be freely downloaded from its official website: *https://root.cern.ch/drupal/*

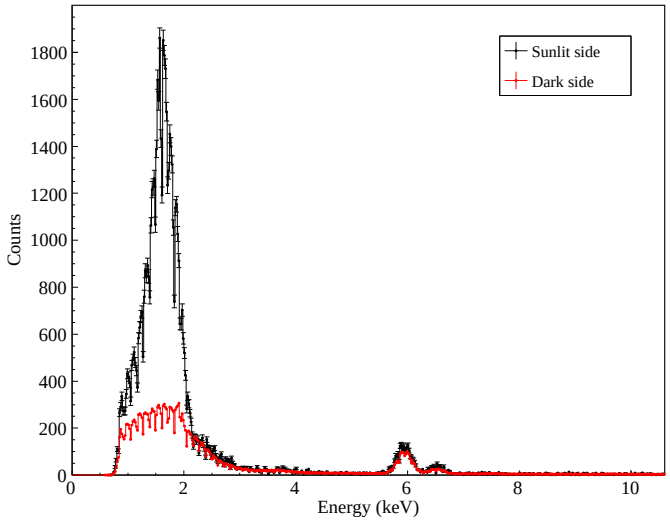


**Fig. 5** Example spectra observed by CE2XRS on the sunlit side (in black points) and on the dark side with solar incident angle larger than $120^\circ$ (in red points) when $T_{\rm solar} = 4$ MK.

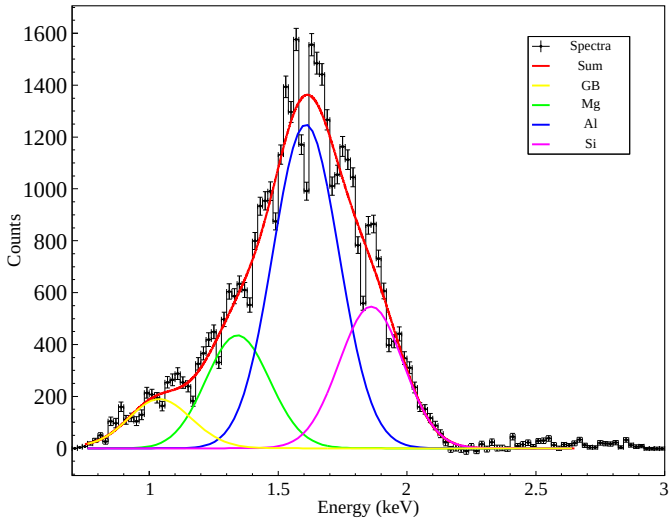


**Fig. 6** The spectra, with electronic noise and cosmic ray induced background subtracted, are fitted by a sum of Gaussian functions for K$\alpha$ lines of Mg (*green line*), Al (*blue line*) and Si (*pink line*), and superimposed on a scattered solar X-ray background in yellow. The line in red is the best-fit result.

CE2XRS and LPGRS are presented as follows. The solar spectra used for CE2XRS derivation in initial analysis are from GOES data, which may result in uncertainty to some extent. The solar activity calibration model that uses CE2XRS Solar X-ray Monitor data will be established in future work. On the other hand, the detection depths of the two techniques are different. X-ray fluorescence is excited by incident solar X-rays at the uppermost surface of lunar regolith. The penetration depth of solar X-rays is $\sim 100$ μm, while the penetration depth of gamma rays is on a centimeter scale.

## 5 CONCLUSIONS

We have described the data analysis procedures in detail for CE2XRS data and have presented the global distributions of Mg/Si and Al/Si on the lunar surface from CE2XRS, which are the first global maps derived from X-ray spectroscopy. Three major geological units (lunar mare, highland and SPA basin) are identified. The results demonstrate that this X-ray remote-sensing technique can also provide important compositional information about the lunar surface.

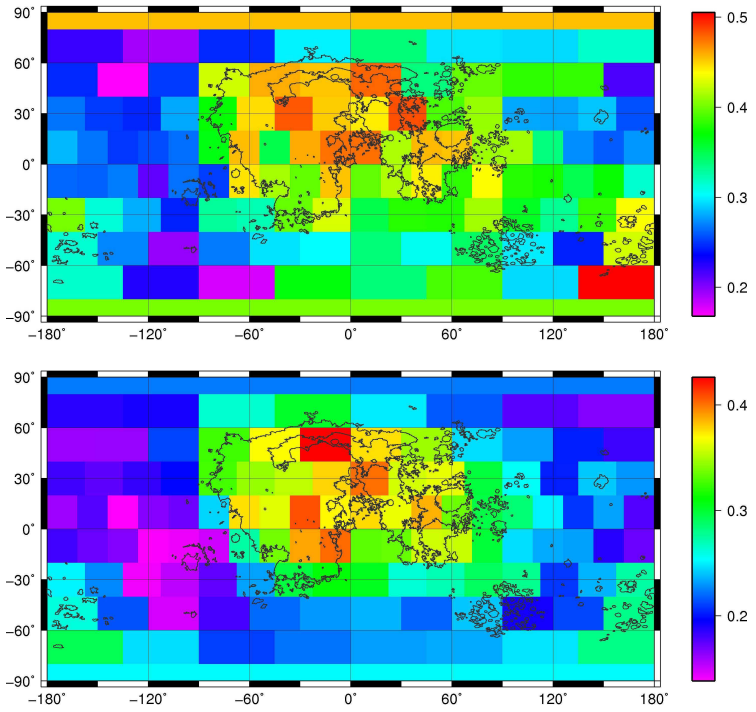


**Fig. 7** The equal-area ($20^\circ \times 20^\circ$) global map of Mg/Si molar ratio distribution on the lunar surface (*Upper*: derived from CE2XRS; *Lower*: derived from LPGRS).

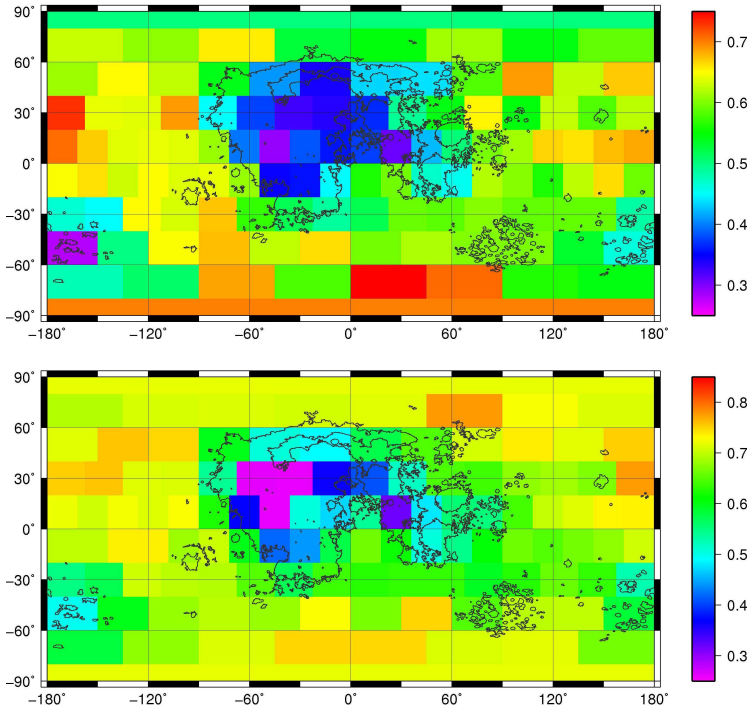


**Fig. 8** The equal-area ($20^\circ \times 20^\circ$) global map of Al/Si molar ratio distribution on the lunar surface (*Upper*: derived from CE2XRS; *Lower*: derived from LPGRS).

**Acknowledgements** We thank Prof. Wang Huanyu, Dr. Peng Wenxi, Dr. Guo Dongya and Dr. Xiao Hong from the Institute of High Energy Physics, Chinese Academy of Sciences, for valuable discussions and help on data analysis. Special thanks go to the Ground Application System of Lunar Exploration, National Astronomical Observatories, Chinese Academy of Sciences for providing the CE2XRS data. This research is supported by the Science and

Technology Development Fund of Macao (Grant Nos. 068/2011/A, 048/2012/A2, 039/2013/A2, 091/2013/A3 and 020/2014/A1) and by the Key Research Program of the Chinese Academy of Sciences (Grant No. KGZD-EW-603).

## References

Adler, I., Trombka, J., Gerard, J., et al. 1972a, Science, 175, 436
Adler, I., Trombka, J., Gerard, J., et al. 1972b, Science, 177, 256
Adler, I., Trombka, J. I., Lowman, P., et al. 1973, Moon, 7, 487
Ban, C., Zheng, Y.-C., Zhu, Y.-C., et al. 2014, Chinese Journal of Geochemistry, 33, 289
Clark, P. E. 1979, Correction, Correlation, and Theoretical Consideration of Lunar X-ray Fluorescence Intensity Ratios, PhD Thesis, University of Maryland
Clark, P. E., & Trombka, J. I. 1997, J. Geophys. Res., 102, 16361
Garcia, H. A. 1994, Sol. Phys., 154, 275
Grande, M., Browning, R., Waltham, N., et al. 2003, Planet. Space Sci., 51, 427
Grande, M., Kellett, B. J., Howe, C., et al. 2007, Planet. Space Sci., 55, 494
Grande, M., Maddison, B. J., Howe, C. J., et al. 2009, Planet. Space Sci., 57, 717
Lim, L. F., & Nittler, L. R. 2009, ICARUS, 200, 129
Mandel'Shtam, S. L., Tindo, I. P., Cheremukhin, G. S., Sorokin, L. S., & Dmitriev, A. B. 1968, Cosmic Research, 6, 100
Narendranath, S., Athiray, P. S., Sreekumar, P., et al. 2011, ICARUS, 214, 53
Nittler, L. R., Starr, R. D., Lim, L., et al. 2001, Meteoritics and Planetary Science, 36, 1673
Nittler, L. R., Starr, R. D., Weider, S. Z., et al. 2011, Science, 333, 1847
Okada, T., Shiraishi, H., Shirai, K., et al. 2009, in Lunar and Planetary Inst. Technical Report, 40, Lunar and Planetary Science Conference, 1897
Ouyang, Z.-Y., Jiang, J.-S., Li, C.-L., et al. 2008, Chinese Journal of Space Science, 28, 361
Ouyang, Z.-Y., Li, C.-L., Zou, Y.-L., et al. 2010a, Chinese Journal of Space Science, 30, 392
Ouyang, Z.-Y., Li, C.-L., Zou, Y.-L., et al. 2010b, Science China Earth Sciences, 53, 1565
Peng, W.-X. 2009, Research on Data Processing Method for Chang'E-1 X-ray Spectrometer, PhD thesis, University of Chinese Academy of Sciences
Peng, W.-X., Wang, H.-Y., Zhang, C.-M., et al. 2009a, Chinese Physics C, 33, 819
Peng, W.-X., Wang, H.-Y., Zhang, C.-M., et al. 2009b, Nuclear Electronics and Detection Technology, 29, 235
Prettyman, T. H., Hagerty, J. J., Elphic, R. C., et al. 2006, Journal of Geophysical Research (Planets), 111, 12007
Swinyard, B. M., Joy, K. H., SMART-1 Team 2009, Planet. Space Sci., 57, 744
Starr, R., Clark, P. E., Murphy, M. E., et al. 2000, ICARUS, 147, 498
Sun, H.-X., Wu, J., Dai, S.-W., Zhao, B.-C., & Shu, R. 2008, Chinese Journal of Space Science, 28, 374
Thomas, R. J., Crannell, C. J., & Starr, R. 1985, Sol. Phys., 95, 323
Trombka, J. I., Squyres, S. W., Brückner, J., et al. 2000, Science, 289, 2101
Weider, S. Z., Joy, K. H., Crawford, I. A., et al. 2014, ICARUS, 229, 254
Weider, S. Z., Kellett, B. J., Swinyard, B. M., et al. 2012, Planet. Space Sci., 60, 217
Yamamoto, Y., Okada, T., Shiraishi, H., et al. 2008, Advances in Space Research, 42, 305